Field thermal monitoring during the August 2003 eruption at Piton de la Fournaise (La Réunion)

Diego Coppola, Thomas Staudacher, Corrado Cigolini

Field thermal monitoring during the August 2003 eruption at Piton de la Fournaise (La Réunion)

Diego Coppola,[1] Thomas Staudacher,[2] and Corrado Cigolini[1]

Received 27 July 2006; revised 15 January 2007; accepted 27 February 2007; published 30 May 2007.

[1] A detailed set of thermal images collected during the last day of the August 2003 eruption of Piton de la Fournaise (La Réunion), clearly revealed several dynamic processes associated with a spatter cone containing a lava pond and feeding a channelized lava flow. Periods of steady effusion were interrupted by brief pulses of lava effusion that closely coincide with peaks in seismic tremor amplitude. The thermal measurements show that roofing of a lava channel during steady effusion and cooling of surface flows decrease thermal radiance in two different ways. Here we show that the decrease in thermal radiance because of channel roofing is not related to a decrease in volcanic activity, as might be interpreted from satellite data. In addition, we introduce a new method of representing thermal data (hereby named ''Radiative Thermogramme'') that successfully describes thermal patterns produced by distinct eruptive processes within the same span of time. This graphic solution can be directly correlated with volcanic field processes and provides a useful tool for interpreting a high number of thermal data in a wide range of volcanic activities.

Citation: Coppola, D., T. Staudacher, and C. Cigolini (2007), Field thermal monitoring during the August 2003 eruption at Piton de la Fournaise (La Réunion), *J. Geophys. Res.*, *112*, B05215, doi:10.1029/2006JB004659.

1. Introduction

[2] Effusive eruptions at Piton de la Fournaise are very common and represent an excellent opportunity to study the thermal features of active lava flows and the associated effusive processes. The thermal analysis of volcanic activity may be performed by remote sensing techniques, since satellite images may easily cover the whole duration of eruption as well as its space distribution [e.g., *Rothery et al.*, 1988; *Pieri et al.*, 1990]. The application of this method has also been used in estimating the size and distribution of thermal areas [*Flynn et al.*, 1994], domes' temperatures and growth [*Francis and Rothery*, 1987; *Kaneko et al.*, 2002], thermal fluxes [*Wright and Flynn*, 2004], and effusion rates [*Harris et al.*, 1997, 2000; *Wright et al.*, 2001]. With few exclusions [cf. *Donegan and Flynn*, 2004], satellite-based methods are inaccurate for obtaining ''detailed'' temperature distributions on selected sites and/or spots. In addition, because of their low temporal resolution, they fail in detecting rapid changes in eruptive activity [*Bailey et al.*, 2006]. However, field-based thermal measurements have been performed by volcanologists by using thermocouples and optical pyrometers. Recently, spectroradiometers [*Flynn et al.*, 1993; *Flynn and Mouginis-Mark*, 1992, 1994], or infrared radiometers [e.g., *Pinkerton et al.*, 2002], were utilized to obtain accurate measurements of effusion temperatures and to constrain some of the physical properties of lavas [*Keszthelyi and Denlinger*, 1996; *Griffiths*, 2000; *Griffiths et al.*, 2003]. Infrared thermometers and radiometers had also been used in monitoring lava lakes [*Harris et al.*, 2005b], strombolian explosions [*Harris et al.*, 1996], fumarole fields [*Harris and Maciejewski*, 2000], and silicic lava flows [*Harris et al.*, 2002].

[3] More recently, the use of handheld thermal cameras increased the possibility of monitoring active volcanoes by acquiring a large amount of thermal data as well as their distribution in space and time. During the 2001 eruption of Mount Etna, *Calvari and Pinkerton* [2004] used a thermal camera to describe the growth and the changes in morphology of the ''Laghetto'' cinder cone. During the 2005 eruption of the same volcano, *Bailey et al.* [2006] monitored cyclic fluctuations of lava volume fluxes within a single flow channel. Additionally, *Harris et al.* [2005a] used thermal data to estimate the variations of the rheological parameters within a lava channel at Mount Etna.

[4] The last paroxysmal eruption of Stromboli volcano gave the opportunity to collect a large amount of thermal data. *Calvari et al.* [2005] detected and monitored craters morphology, fracture systems, and their dynamic behavior during the different phases of the eruption. Similarly, lava tube development and lava field emplacement were recorded. *Harris et al.* [2005c] introduced a new method for obtaining daily estimates of the effusion rates from images-derived thermal fluxes. During the 2005 eruption on Mt. Etna, *James et al.* [2006] first used photogrammetric and machine vision techniques to combine spatial data with thermal imagery to obtain a three-dimensional spatial distribution of flow profiles and flow rates. Although, the use of ground-based thermal cameras becomes more wide-

[1] Dipartimento di Scienze Mineralogiche e Petrologiche, Università di Torino, Torino, Italy.
[2] Observatoire Volcanologique du Piton de la Fournaises, Institut de Physique du Globe de Paris, La Réunion, France.

0148-0227/07/2006JB004659$09.00

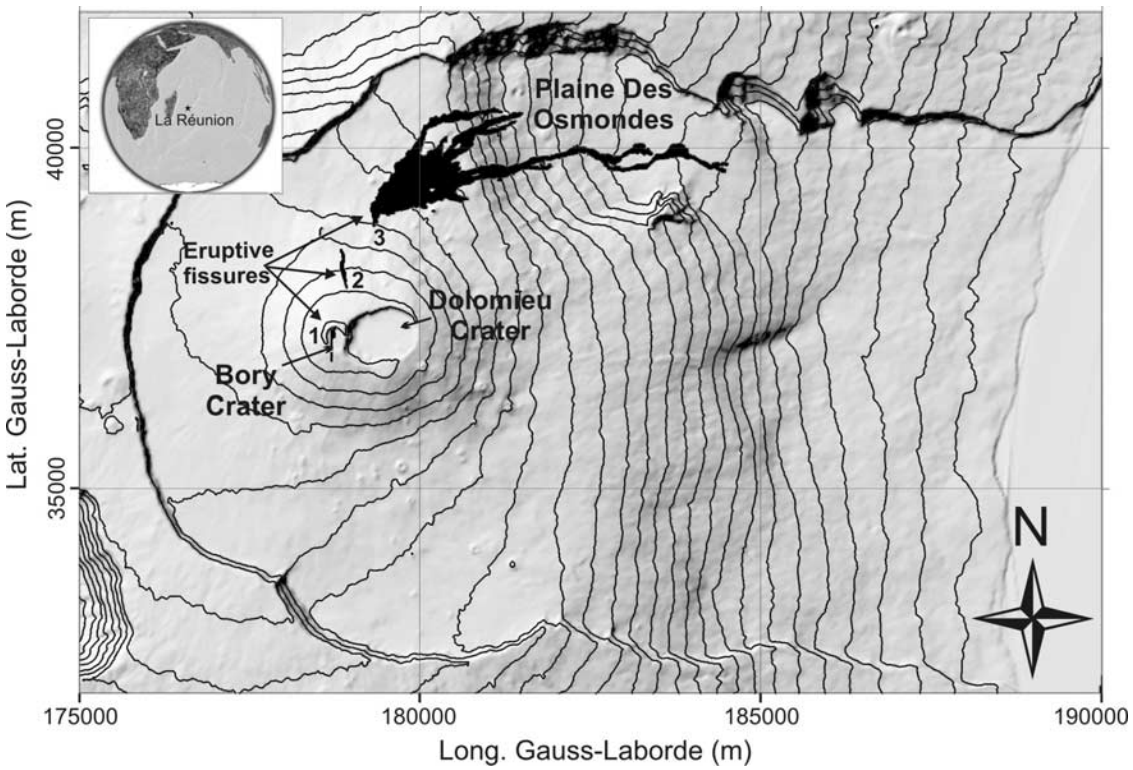

Figure 1. Location of the August 2003 eruption. The first fissure opened within the Bory Crater and was followed by two more fissures on the northern flank of the volcano. The northernmost fissure produced a 5-km long lava field within five days of activity.

spread, only few works focus their attention on the temperature distribution on lava surfaces. *Wright and Flynn* [2003] illustrated that the complex temperature distribution on an active pahoehoe flow field can lead to significant errors in estimating subpixel features from satellite images (because of their relatively low resolution).

[5] In an earlier paper on the May to July 2003 eruption of Piton de la Fournaise [*Coppola et al.*, 2005], we showed that the temperature distribution over the lava field is composed of multiple thermal components, which are in turn related to different flow-units (whose style of emplacement and cooling histories can be eventually reconstructed).

[6] In this paper, we present new thermal data on the August 2003 eruption of Piton de la Fournaise by using a forward looking infrared (FLIR) thermal camera. We report conventional analysis on the basis of the average temperature time series within several selected fields of view (FOV). In addition, we propose a new methodology for thermal monitoring on the basis of the evolution of the Temperature Distribution (TD) within the selected sites. These undergo morphological changes during the ongoing eruption. Particularly, we concentrated our efforts in monitoring the effusive activity in the proxymal area and in decoding the cyclic pulses of lava effusion. Finally, we attempted to correlate these pulses with the peaks in the recorded seismic tremor.

2. The August 2003 Eruption

2.1. Recent Activity of Piton de la Fournaise

[7] On March 1998, Piton de la Fournaise entered into a new cycle of recurrent volcanic eruptions after nearly 6 years of rest [*Staudacher et al.*, 2001]. From 1998 to the present day, more than 20 eruptions have been recorded. The observed eruptive events has been subdivided into two "eruptive styles" [*Vlastélic et al.*, 2005]:

[8] 1. High-flux eruptions of "oceanites" (picritic lavas formed upon flushing the slurry from a dykes [cf. *Albaréde et al.*, 1997]) from the rift zones of the volcano;

[9] 2. Low-to-intermediate flux eruptions of steady state Basalt (named SSB by *Albaréde et al.* [1997]) from the summit and the radial fracture zones.

[10] The August 2003 eruption (Figure 1) represent the twelfth eruptive episode occurred on Piton de la Fournaise since the beginning of the last cycle [*Peltier et al.*, 2005, 2006] and can be classified as a transitional case between intermediate and high flux eruptions defined by *Vlastélic et al.* [2005].

2.2. Chronology of the Eruption [All Times are Given in Coordinated Universal Time (UTC)]

[11] Only a few days after the end of the 30 May to 08 July 2003 summit eruption [cf. *Coppola et al.*, 2005], volcanic seismicity slightly resumed on 12 July 2003. This was coupled with a gradual inflation of the volcanic edifice that strongly increased on August 22. At this time, a seismic crisis begun below the summit of the volcano [*BGVN*, 2003] at a level ranging between 200 and 800 m above sea level. The seismic crisis was accompanied by an important summit inflation (up to 30 cm) centered beneath the Dolomieu crater. Vertical injection of magma lasted only 20 min (about 1.5–2 m/s) [*Peltier et al.*, 2005], and at 17:20 on 22 August 2003, a first eruptive fissure opened in the

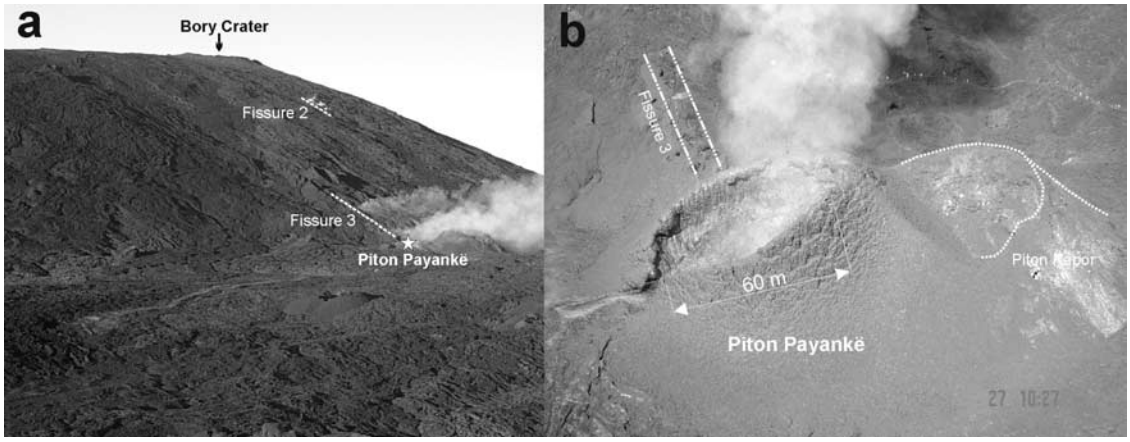

Figure 2. (a) View of the northern flank of Piton de la Fournaise on 23 August 2003. The star at the base of the third fissure indicates the location of Piton Payankë. On its right is visible the Piton Kapor, the main cone of the 1998 eruption; (b) By 27 August, Piton Payankë has grown over Piton Kapor (photos by Th. Staudacher).

Bory crater (adjacent to the Dolomieu crater, on the W). This event was followed by a lateral dike intrusion (about 0.2 m/s) [*Peltier et al.*, 2005], and at 18:10, it was followed by the opening of a second fissure on the N flank at the altitude of ~2450–2470 m a.s.l. Both fissures were active for a short time (fissure 1 and 2, in Figure 1).

[12] At 19:31 of that day, a third and last fissure opened on the N flank at 2200 m (fissure 3 in Figure 1). On the basis of three independent ASAR interferograms, *Froger et al.* [2004] indicated that the opening of these three fissures was associated to the intrusion of a 57° eastward dipping dyke, with a base lying around 1520 m a.s.l.

[13] The lowermost segment of the third fissure was located only few tenths of meters east of Piton Kapor, the main cone formed during the 198 days of activity of the 1998 eruption [*Staudacher et al.*, 2001].

[14] During the first hours of activity an intense odor of sulphur was reported by people living several kilometers far from the eruption site. This led us to suggest that the initial stages of the eruption were accompanied by sustained degassing. During the night, the effusive activity gradually shifted at the base of the third fissure (Figure 2a), and in the morning of 23 August, a new growing spatter and scoria cone (named Piton Payankë) was observed (Figure 2b). Field observations reported that lava fountains 15–20 m high were active within the forming cone that, in turn, was feeding a new and wide lava field. In this proximal sector, a very fluid and degassed lava was flowing on very gentle slope and progressively constructed a pahoehoe channel-fed flow field that developed on the northeast direction for about 2 km. Some distal portion of this flow field reached the steeper zone contouring the "Plaine des Osmondes" and evolved into narrow distinct aa branches (Figure 1). On 24 August, the activity within Piton Payankë (whose dimensions reached those of the neighbor Piton Kapor) showed a gradual decrease in lava fountaining (~5–10 m high) thus causing the aa flow fronts on northeast to slow down and eventually stop. The effusion rates estimated in the morning of 25 August ranged from 5 to 10 m^3/s, but later in the afternoon, the intensity of the activity inverted its trend and started to grow again. This trend was also observed on the intensity of volcanic tremor (RSAM, real-time seismic-amplitude measurement; Figure 3a) recorded by the seismic network of the observatory and by the radiative thermal flux (Figure 3b) detected remotely by the MODVOLC algorithm (http://modis.higp.hawaii.edu/) developed by the moderate-resolution imaging spectroradiometer (MODIS) Alert Team [*Wright et al.*, 2002, 2004]. Simultaneously, with the increase of the activity, more and more olivine were found in the lava, forming "oceanites" at the end of the eruption.

[15] During the following two days, more vigorous and intermittent fountaining (15–50 m high) has been observed within Piton Payankë, accompanied with the formation of a lava pond. The resumed intense activity at the vent led to the emplacement of a new major lava flow located onto the eastern side, slightly diverging from earlier flows. The new flow quickly reached the "Plaine des Osmondes" and developed several aa branches, the longest advanced for a distance of about 5 km (Figure 1). In the morning of 27 August, field estimates indicated that the effusion rates increased to about 20–30 m^3/s, but later in the evening (17:54 UTC), the eruption abruptly ceased (following a phase of vigorous fountaining that lasted for about 30 s).

[16] The eruption produced a composite lava field of olivine-rich basalt that covered an area of about 1.6 km^2. GPS measurements on the whole lava field indicated that a total volume of lava of about 6.2 Mm^3 was produced with an average eruption rate of 13 m^3/s [*Staudacher et al.*, 2007].

3. Structure and Activity of the Vent Area on 27 August 2003

[17] The persistent activity at the base of the third fissure led to the growth of an elliptical spatter and scoria cone (about 100 m long and 30 m high, with average external flank-slope of 45°), containing a lava pond with a diameter of about 50 m. On the western and southern sides, this pond was delimited by the crater walls, whereas on the eastern side, the lava was prevented from overflowing just by a

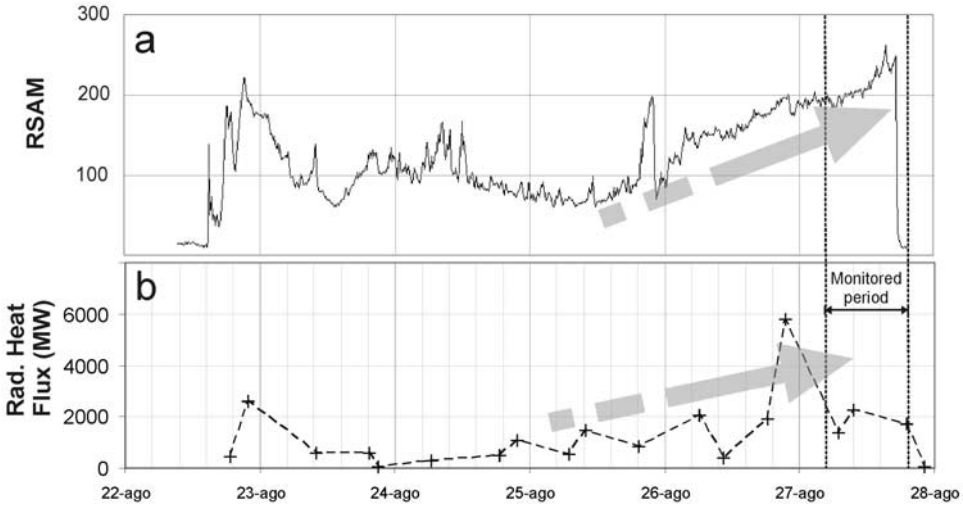

Figure 3. Seismic and thermal activity during the eruption. (a) RSAM recorded by the ''La Soufriere'' seismic station showing the increasing trend in tremor amplitude during the last days of eruption; (b) Radiative heat flux calculated from the MODVOLC data, following *Wright et al.* [2004]. Seismic data were provided by the Observatoire Volcanologique du Piton de la Fournaise; MODIS data were provided by HIGP-MODIS Thermal Alert Team.

small barrier, about 0.5–1.5 m above the free surface of the lava pond (i.e., nearly 9 m above the adjacent lava field). A sketch of the vent area is reported in Figure 4. On the basis of field observations, the volcanic activity observed on 27 August can be subdivided into two phases, a stable and persistent effusion of lava (steady state effusion) which was from time to time interrupted by rapid changes of the lava level within the pond, hereby named ''effusive pulses''. We will therefore focus our analysis on these two phases.

3.1. Steady State Effusion

[18] During steady state effusion (Figure 4a), the lava-pond was confined within the cone by its natural eastern barrier. Lava fountains reached a height of 15–30 m, producing abundant spatters, scorias, and lapilli that fell back to the pond or were deposited onto the external flank of the cone as well as on the adjacent lava field (Lpf). Despite continuous degassing and fountaining, the free surface of the pond was substantially stable about 0.5–1.5 m below the barrier.

[19] A steady drainage of the lava pond occurred through a main breakout (Bk) located at the base of the cone (about 30 m on the east) which, in turn, fed a main lava channel (Figure 5). Within the first meters, the channel developed onto a nearly flat slope (<5°), before reaching a steeper sector (about 30°) beyond 40 m from the cone. Where the lava was flowing onto the gentler slope, the channel was about 20 m wide, and we estimated a surface velocity of 0.4 ± 0.1 m/s. These measurements, coupled with those performed within the empty channel (with a depth of 2–3 m) after the ceasing of the eruption, allowed us to estimate a channel lava supply rate of about 14 ± 6 m^3/s.

[20] The stable flux produced by the Bk led to the growth of a rooted crust according to the mechanism described by *Peterson et al.* [1994]. By citing his words, this process occurs when ''a thin film of plastic lava adhere to the levees because of solidification and growth toward the centre and downstream, up to a complete closing of the channel''. In Figure 4a, the forming roof within the lava channel is indicated with the abbreviation Rf. During this process, the portion of stable roof insulating the lava from the Bk moved downstream for more than 30 m. At the same time, the flow field in proximity of the cone was continuously affected by the formation and the disappearance of minor ephemeral vents (Ev), which produced short-lived and small lava tongues (max. 20 m long).

3.2. Effusive Pulses

[21] The steady state effusion was cyclically interrupted by quick changes of the lava level within the summit pond, hereby defined as ''effusive pulses''.

[22] During these episodes (Figure 4b), several simultaneous phenomena were observed in the vent area. The onset of these dynamic pulses produced an overpressure within the lava pond, quickly transferred to the main Bk (toward the tube system) thus producing an increase of the stream velocity and interrupting the roofing process. The pulses caused the lava pond's free surface to rise up to the barrier level followed by thin pahoehoe overflows (O_P) that advanced for few tens of meters with a velocity of 0.12–0.15 m/s before cooling and stopping. These processes were accompanied by an increase in the fountain height (up to 30–50 m) which lasted for a few minutes before returning to a more stable level (15–30 m). At the same time, the base of the cone inflated and the lava squeezed up from the preexisting and/or new ephemeral vents (Ev). Once the overpressure has been transferred downstream, it produced channel overflows (O_{Ch}) that spread laterally with a rate of 0.15–0.20 m/s.

[23] Our hypothesis (discussed later) is that the observed pulses were associated to the occurrence of ''gas pistons events'' [*Swanson et al.*, 1979; *Tilling*, 1987], a degassing mechanism commonly observed at Kilauea volcano [*Johnson et al.*, 2005].

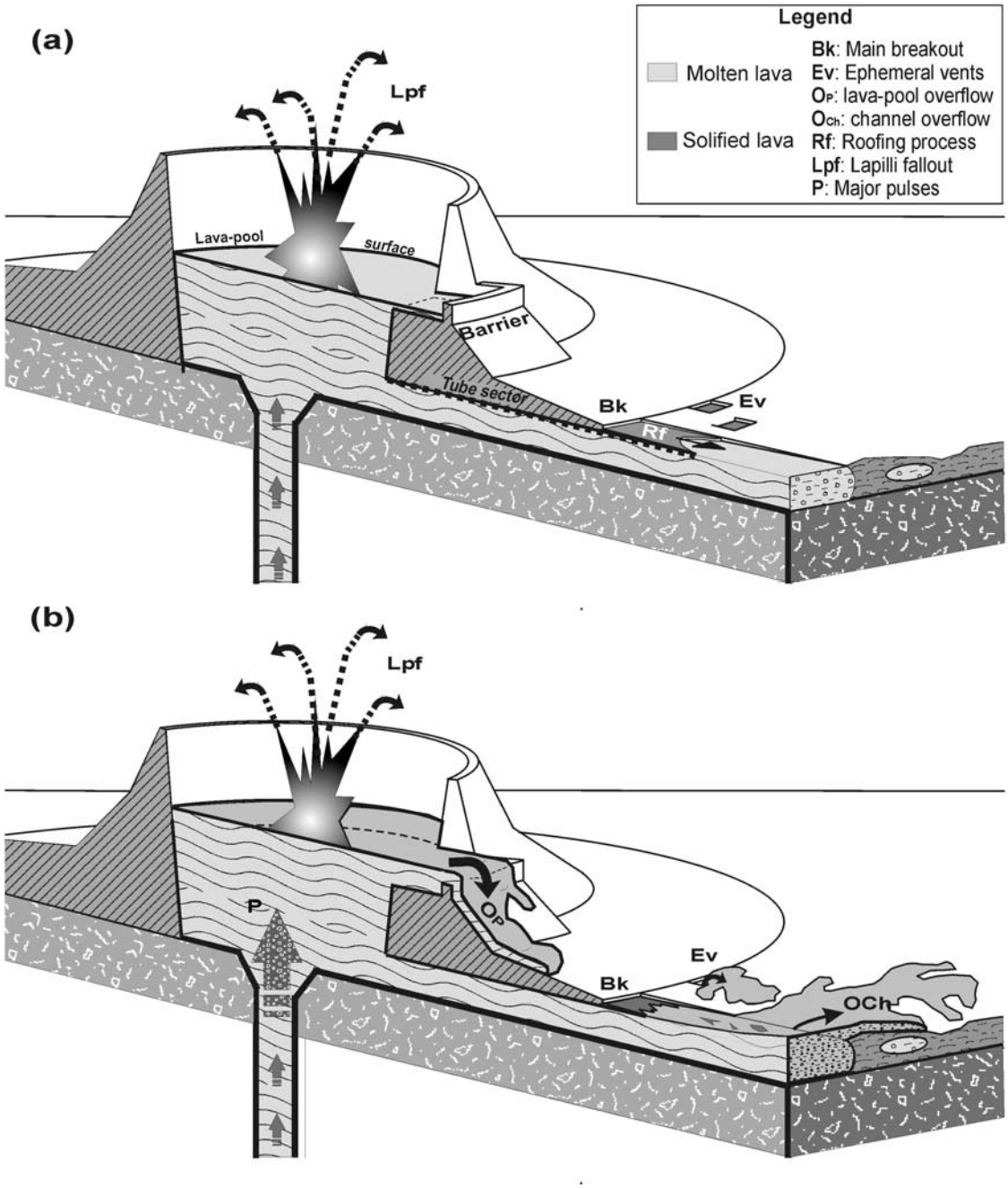

Figure 4. Sketch map of the near-vent structure and activity. (a) During steady state effusion, the lava pond is delimited by a barrier on the eastern side. Drainage occurs from a breakout at the base of the cone; (b) Dynamic pulses caused pond's and channel's overflows. Ephemeral vents occasionally developed at the base of the cone.

[24] During our monitoring period (see next chapter), a total of six major pulses were observed. They occurred at time intervals ranging from 60 to 140 min and generated cyclic overflows both within the pond and/or the upper part of the channel. We estimate that the ''free surface'' of the lava pond (approximately 1960 m^2) rose about 1–1.5 meters in less than 2 min (thus adding about 1960–2940 m^3 to the pond). Therefore the dynamic pulses increased the effusion rate nearly instantaneously of about 20.4 ± 4.1 m^3/s, which is approximately the same order of magnitude of the averaged channel flow rate during the steady state conditions.

[25] We also recognized several ''minor pulses'' that did not trigger overflows of the lava pond but simply produced the squeezing of lava from the ephemeral vents as well as interrupt the roofing process and produced small channel overflows.

[26] The ceasing of the effusion was accompanied by the total draining of the ponded lava coupled with a substantial deflation at the base of the cone. We estimated a vertical

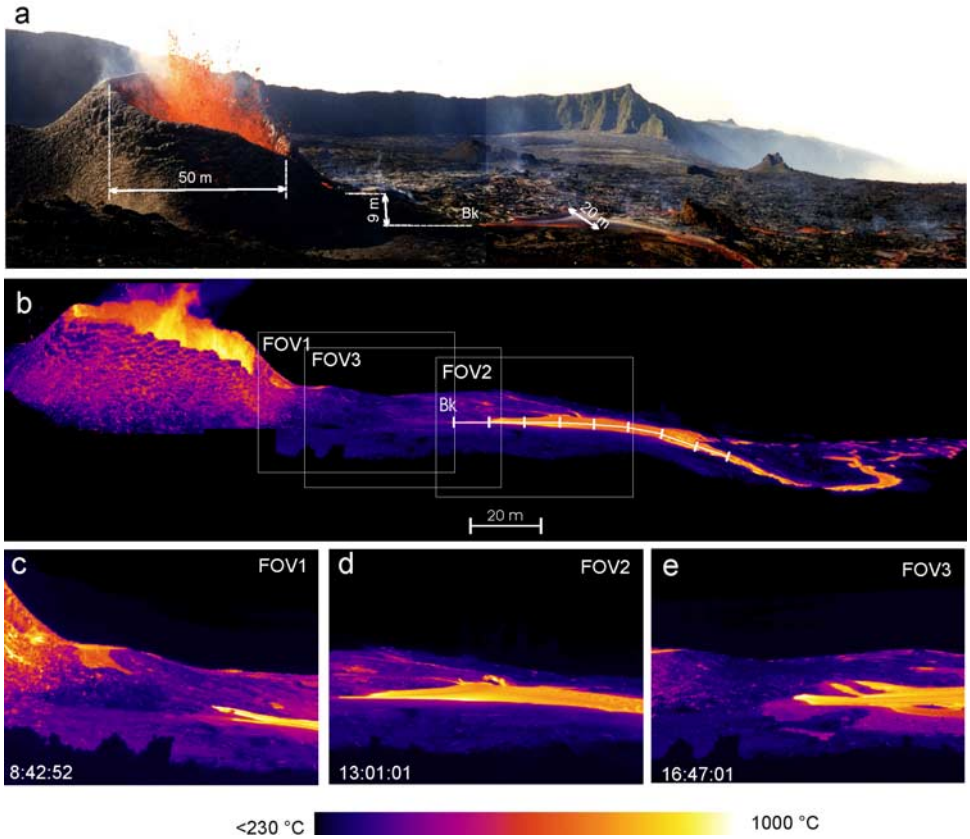

Figure 5. (a) Optical image of the vent area, the lava is flowing through Bk into the main lava channel that is forming the lava field; (b) Thermal image of the vent area, three different FOV describe the activity at the base of Piton Payankë; (c) FOV1 started on 27 August 2003 at 08:42:52 and was focused on the lava pond's overflows and ephemeral vents; (d) FOV2 started at 13:01:01 and was focused on the activity within the channel; (e) FOV3 started at 16:47:01 and was again focused on the pond's overflows and ephemeral vents.

displacement of this structure of about 1.25 m, which occurred approximately in 15 min (8.33 cm/min).

4. Technical and Analytical Methods

[27] Thermal monitoring was concentrated on the near-vent activity. It was performed by collecting sequences of thermal images focussing at the upper part of the channel connecting to the cone (Figure 5). We used a FLIR ThermaCAM PM695 that acquires images of 320 × 240 pixels with three possible ranges of temperature [cf. *Calvari et al.*, 2005]. We used the higher extended range of temperature that allowed us to detect temperature from 217.2° to 1500°C. The images were recorded every 2 min and stored in a PCMCI card for further analysis.

[28] The camera (equipped with a 24° objective) was located at about 140 m from the vent, which matches a FOV of nearly 60 × 45 m, where each pixel represents an area of 0.0361 m^2 (0.19 × 0.19 m). *Bailey et al.* [2006] have shown that these conditions are satisfied when the camera viewing is perpendicular to the target, which does not always occur during field work. Thus, geometric corrections are necessary to have reliable estimates of the pixel area. To simplify the complex geometric adjustment needed to correct the effects of different view-angles and different distances within the same FOV, we considered a uniform angle of view of about 10° (i.e., the angle of intersection between the FLIR's line of sight and the channel surface) and a constant distance of 140 m (average distance between the camera and the center of the channel). This correction produced pixels of 1.08 m × 0.19 m each, so that 2000–5000 m^2 of the lava field (at $T_{PIX} > 217.2$°C) were analyzed in each image.

[29] According to *Ball and Pinkerton* [2006], the geometric adjustment has to be accompanied with a correction of the "pixel temperature" because of the influence of several parameters on the radiance detected by the instrument. As explained by the same authors, the errors due to the changes in the emissivity and roughness of the basaltic lava surfaces can affect the pixels temperature of about 15°C. Additional perturbations can be due to the atmospheric attenuation (about 75°C for a 250-m long atmospheric path at relative humidity of 50%) to the viewing distance (up to 200°C, for viewing distance of 250 m) and to the viewing angle (about 1°C/degree for viewing angle major than 30°).

[30] In our case, we assumed that roughness and emissivity (for the basalts of Piton de La Fournaise we assume $\varepsilon = 0.967$; [*Coppola et al.*, 2005]) did not change during our

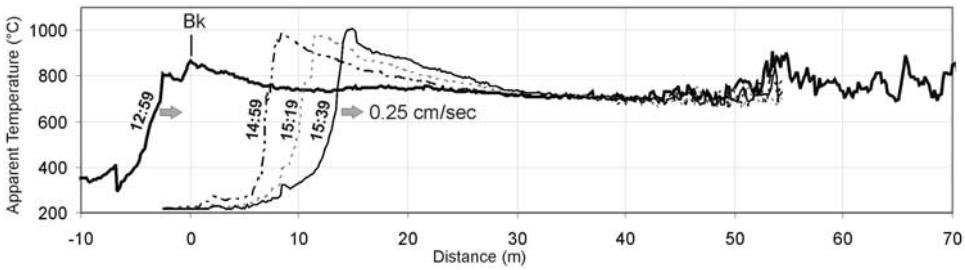

Figure 6. Thermal profiles over the main lava channel reported in Figure 5b. The advancing stage of Bk can be detected by the "moving" temperature peak (shifting toward the right side). The roofing process caused strong insulation upstream of Bk, whereas the change in terrain slope is marked by increasing temperature fluctuations (at about 50 m from the initial position of Bk).

monitoring, so that the errors produced by these factors were stable (about 2–7% of the detected temperature).

[31] We simplify the temperature correction in the light of the cited view-distance (140 m) and view-angle (10°) and assuming a uniform humidity of 25%. Since these parameters are uneven within the thermal images and can change during the monitoring period, we reported the pixel temperature as an "apparent temperature" as postulated by *Johnson et al.* [2005]. This explains why during our thermal monitoring, we recorded a maximum apparent temperature of 1105°C (cf. Figure 13a), a value about 45–70°C lower than the typical effusive temperatures measured on Piton de la Fournaise (1150–1170°C) [*BGVN*, 1998, 2000, 2001].

5. Thermal Monitoring

[32] Thermal monitoring started on 27 August at 08:42 (all times are UTC), then, after more than 10 hours of records, the eruption stopped suddenly at 17:54.

[33] The whole analyzed sequence has been subdivided into three sequential periods named FOV1, FOV2, and FOV3, respectively (Figure 5b). During each of these periods, we collected thermal data for a specific field of view.

[34] The first field of view (FOV1, from 08:42:52 to 12:48:52) was focused on the barrier of the lava pond and on the Bk at the base of the cone (Figure 5c).

[35] FOV2 (from 13:01:01 to 16:45:01) looked few meters downstream of the above field of view and was focused toward the moving breakout and on the lava channel that developed from it (Figure 5d). Finally FOV3 (from 16:47:01 to 19:33:01) shoots back to the barrier of the pond and to the activity occurring at the breakout, including the Ev at the base of the cone (Figure 5e).

[36] Between the end of FOV1 (12:48:52) and the beginning of FOV2 (13:01:01), we interrupted the automatic acquisition of images for a few minutes to be able to collect a complete thermal view of the vent area (Figure 5b).

[37] We first used the "apparent temperature" profiles to measure the intensity and the spatial evolution of the roofing process. Then we treated the averaged temperatures (Tave) recorded within the FOVs during the dynamic evolution of the eruption. Finally, a new and detailed analysis has been conducted on the temperature distribution (TD) together with the radiative power distribution (QD). This approach led us to the construction of a three-dimensional time series that we named "Radiative Thermogramme", abbreviated as ("RadTherm") which takes into account the evolution of the radiative power distribution (QD) during the sequence of the observed phenomena.

5.1. Temperature Profiles and Roofing Growth Rate

[38] In Figure 5b, we report the thermal view of the near-vent area collected at 12:59 of 27 August 2003. A thermal profile is drawn along the central part of the main channel and is plotted onto Figure 6 (black thick line). The lava flowing out of the Bk was exposed to the atmosphere and started to cool because of the quick heat loss in the initial seconds of exposure [*Keszthelyi and Denlinger*, 1996]. The progressive decrease in temperature is particularly evident within the first 10–15 m. At a distance beyond 40 m, the thermal profiles become more variable likely because of the disruption of crust brought on by flowing along steeper slope.

[39] Three additional thermal profiles (they involve only FOV2) were obtained later at 14:59, 15:19, and 15:39, respectively (Figure 6, thin lines). They indicate a "marked insulation" taking place during the roofing process just a few meters before the Bk which is moving downstream (grey arrow). As mentioned earlier, the roofing process was quite rapid during the reported steady state effusion, and we estimated a downstream growth rate of about 0.25 cm/s, which is about 0.6% of the channel surface velocity. In addition, we estimate that during steady state conditions, the decrease of the channel surface that was in contact with the atmosphere occurred at a rate of about 0.05 m^2/sec. At this rate, a hypothetical lava channel 10 m wide and 400 m long could be completely insulated in one day of steady effusion.

5.2. Temperature Versus Time

[40] The observation of the thermal images, coupled with the analyses of the averaged temperatures within the FOVs (T_{ave}), allowed us to associate most of the observed phenomena to a typical thermal trend.

[41] The occurrence of major pulses (named P1 to P6) produced a drastic increase of T_{ave}, principally because of the emplacement of the overflows (cf., grey arrows in Figure 7). Differently, the minor pulses (white small arrows) did not produce pond overflows but only the opening of ephemeral vents, detected as smaller thermal peaks (cf., white arrows in Figure 7). This minor thermal anomalies are less pronounced than those produced by the main pulses, and without the observation of the original images, they can be confused with similar spikes of T_{ave} recorded during

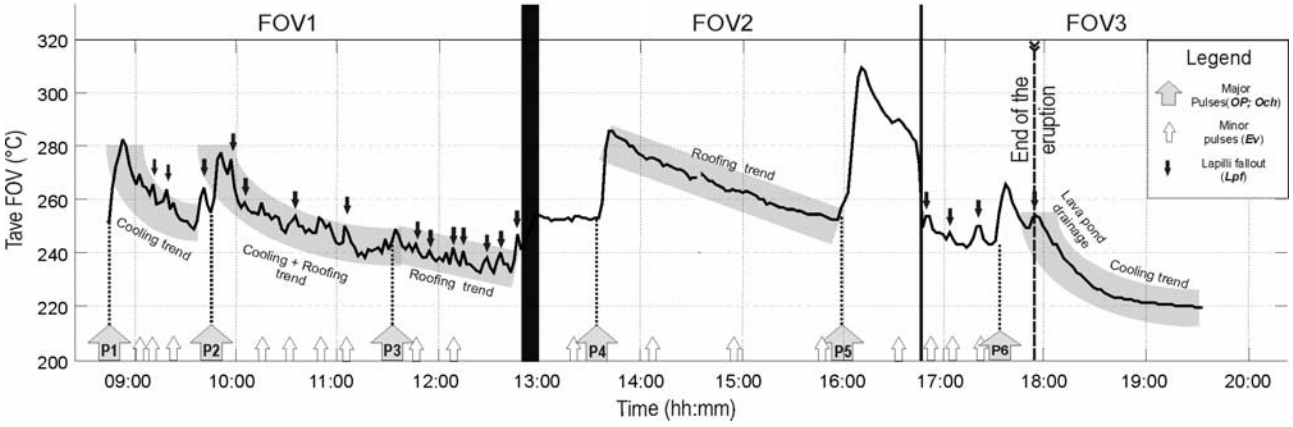

Figure 7. Time series for the FOV's average temperature. Major pulses (P1 to P6) produced clear thermal anomalies because of lava pond overflows, channel overflows, and formation of ephemeral vents. Two different trend of decreasing temperature may be distinguished, the nonlinear decrease is associated to cooling, and the linear decrease is due to the roofing process.

lapilli, spatter, and scoria fall-outs (Lpf) within the FOV (cf., black arrows in Figure 7).

[42] Once the overflows were no longer fed by the new lava (coming from the pond), they started cooling relatively rapidly (see Figure 7, FOV1 and FOV3). This phenomenon would cause a "nonlinear" decrease of the average temperatures (hereby named "cooling trend") previously observed in Hawaiian basalt [*Hon et al.*, 1994]. In contrast, when the flow rate approaches steady state conditions (in the time span between two pulses), the regular propagation of the roof downstream limited the exposure of the hot surface to the camera, thus producing the nearly "linear" decrease of the average temperature (roofing trend) despite a constant supply rate (i.e., after pulse P4 in Figure 7). These two trends are both characterized by a lowering of the average temperature within the FOV, but as mentioned and discussed, they result from two different key-process, cooling and roofing. However, these two processes can occur at the same time, and the resulting thermal signal is a mixing between the two trends (i.e., after the pulse P2; Figure 7).

[43] Following pulse P6, the end of the eruption produced the last peak within the FOV3 because of the spectacular fountains observed on the field in the last seconds of activity. This last episode was followed by the drainage of the lava within the pond that outflowed from the Bk and the Ev with the consequent deflation of the base of the cone.

5.3. Temperature Distribution and Radiative Power Distribution

[44] A different and more useful way to visualize the thermal data is represented by analyzing the TD of single thermal images. The TD is a frequency histogram representing the fractional area (f) occupied by the surface at discrete classes of temperature. The whole range of recorded temperatures (from 217° to 1105°C) was subdivided into bins of 10°C each. The number of pixels within each bin was automatically counted and plotted as fractional area (f).

[45] In the example of Figure 8, the thermal image, recorded at 13:01 (Figure 5d), shows a TD composed by two main components. The presence of the channel, in which the hot flowing lava is continuously exposed at the surface, is represented by a great number of pixels with temperatures higher than 630°C. The adjacent cooling lava field is represented by an increasing exponential trend in the cooler sector of the TD. By analyzing the whole sequence (Figure 9), we observed that this bimodal distribution is always maintained so that we defined the high temperature region (T > 630°C) of the TD as the "active region" since these components were generally related to the hot moving lava. In contrast, the cooler surfaces (T < 630°C) were associated to stationary surfaces and were only allowed to cool within the FOV. These are represented by those thermal components in the "stationary region" of the TD.

[46] In terms of energy flux, the TD can be regarded as a distribution of the radiative heat flux (QD) lost by the surface (Figure 8b). By knowing the total analyzed area, the net radiative heat flux lost in each class of temperature (Q_{RadCL}) can be calculated as follows:

$$Q_{RadCL} = f_{CL} A_{TOT} \sigma \varepsilon T_{CL}^4 \quad (1)$$

where Q_{RadCL} is in watts, f_{CL} is the fractional area at the class temperature T_{CL}, A_{TOT} is the total analyzed area (in m^2), σ is the Stefan Boltzmann constant (5.67×10^{-8} W/m^2 K^4), ε is the emissivity, and T_{CL} is the class temperature (in °K).

[47] The integral of the TD illustrated in Figure 8a represents the total analyzed area (A_{TOT}) within the FOV at temperatures higher than 217°C (2512 m^2), whereas the integral of the QD represents the total radiative power loss by the same monitored portion of flow field (Q_{Rad} = 59.2 MW; Figure 8b).

[48] We now attempt to show the dynamic effect of the first pulse (P1) on the TD and the related QD (Figure 10).

[49] We focused our analysis both on the entire FOV as well as on selected active areas named sFOV. These were looking at the barrier of the lava pond (sFOV1a) and at the main Bk at the base of the cone (sFOV1b).

[50] Before the pulse P1, the thermal activity of the main Bk, together with an older pond overflow (O_{P0}), produced on the TD two principal components in the "active" and "stationary" regions, respectively (Figure 10a). The pulse onset produced the overflow O_{P1} as well as the opening of

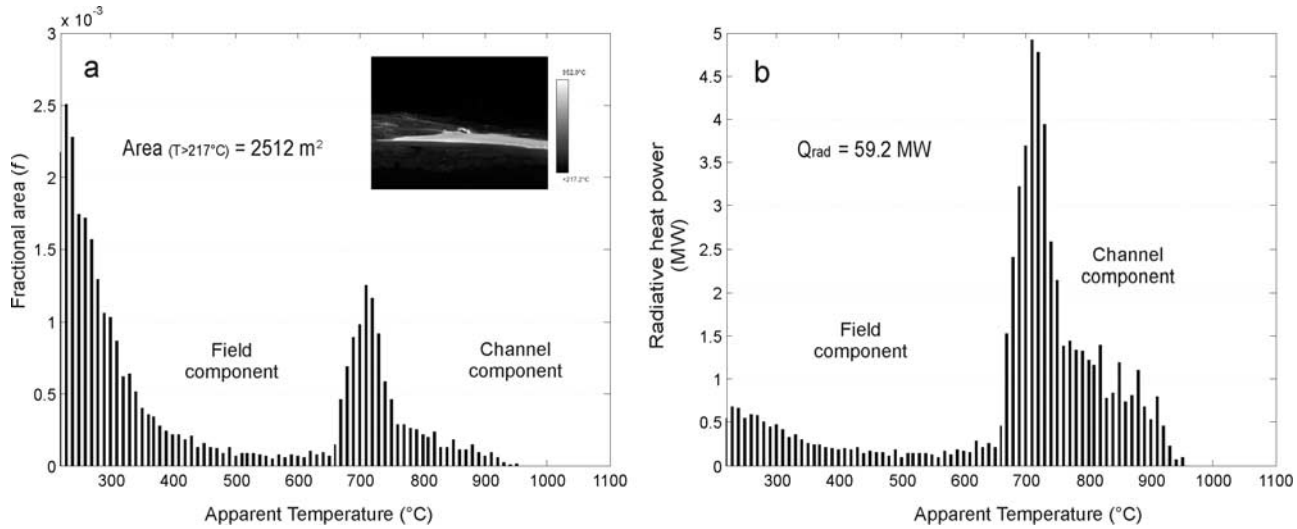

Figure 8. (a) TD of the image collected at 13:01:01. Main components are related to channel surface, and adjacent lava field; (b) Radiative heat power distribution (QD) of the cited image. The channel component is much more evident because of the higher temperature of its surface.

a new Ev, both represented by new high-temperature components that overlap the Bk component within the "active region" (Figure 10b). The cooling of the overflow produced a gradual shifting of its thermal signature that moved toward lower temperature located in the "stationary region" (Figure 10c). After 28 min, the overflow component is being absorbed by the background, whereas the Ev + Bk activity has increased and is represented by a stronger thermal component in the active region (Figure 10d).

[51] Coeval anomalies are visible on the radiative power distribution (QD). Pulse P1 led to the growth of the radiative heat loss from about 46.8 MW (Figure 10a) up to 70–75.3 MW (during the overflow; Figure 10b and 10c, respectively). After the cooling of the overflow, the radiative power within the field of view has decreased to a value of about 51.7 MW (Figure 10d), according to an activity of the main Bk and the new Ev higher than before the pulse P1.

5.4. Radiative Thermogramme (RadTherm)

[52] To be able to better visualize the evolution of the QD with time, we produced a graphic solution that we hereby name "Radiative Thermogramme" (RadTherm). The QD of all the images are placed side by side; the apparent temperature bins (on *Y* axis) are plotted versus time (*X* axis), and the radiative power at the surface relative to each class of temperature is plotted onto the *Z* axis (Figure 11). Into the *XY* section, the intensity of the radiative power is represented according to a logarithmic color scale.

[53] Since the field of view changed during the period of monitoring, we analyzed separately the RadTherm for each single FOV.

[54] In Figure 12a, we represent the RadTherm of FOV1. The hotter surfaces (active region) appear in the upper part of the plots. The amount of radiative thermal flux lost by these surfaces is related their abundance within the FOV. During the steady effusion periods, the moving lava components were essentially related to the main Bk and the Ev. The occurrence of major pulses depicts a rather instantaneous increase of the intensity of the thermal components observed within the active region because of the ponds' overflow through the barrier. However, the best graphical evidence for the occurrence of magma pulses is the high-energy curves generated by the lava overflows that cools and becomes stationary. These curves (named OP) indicate the migration of thermal components toward lower temperatures as previously illustrated in Figure 10.

[55] The intensity of these "cooling-curves" is related to the area occupied by the active "flow units," therefore the low-energy curve produced by the squeezing of lava from Ev represent the effects of the associated minor pulses. Differently, the slope of these curves is proportional to the

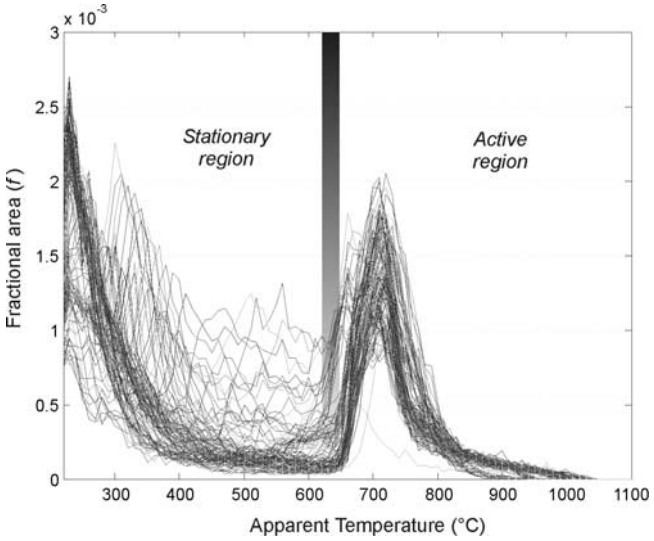

Figure 9. Overlapping of the TD for the whole sequence of images. Two distinct sectors can be observed, the lower temperature region represents "stationary" surfaces that cools within the FOV whereas the high-temperature region represents "active" lava surfaces that are moving. The transition between the two zones occur at about 630°C.

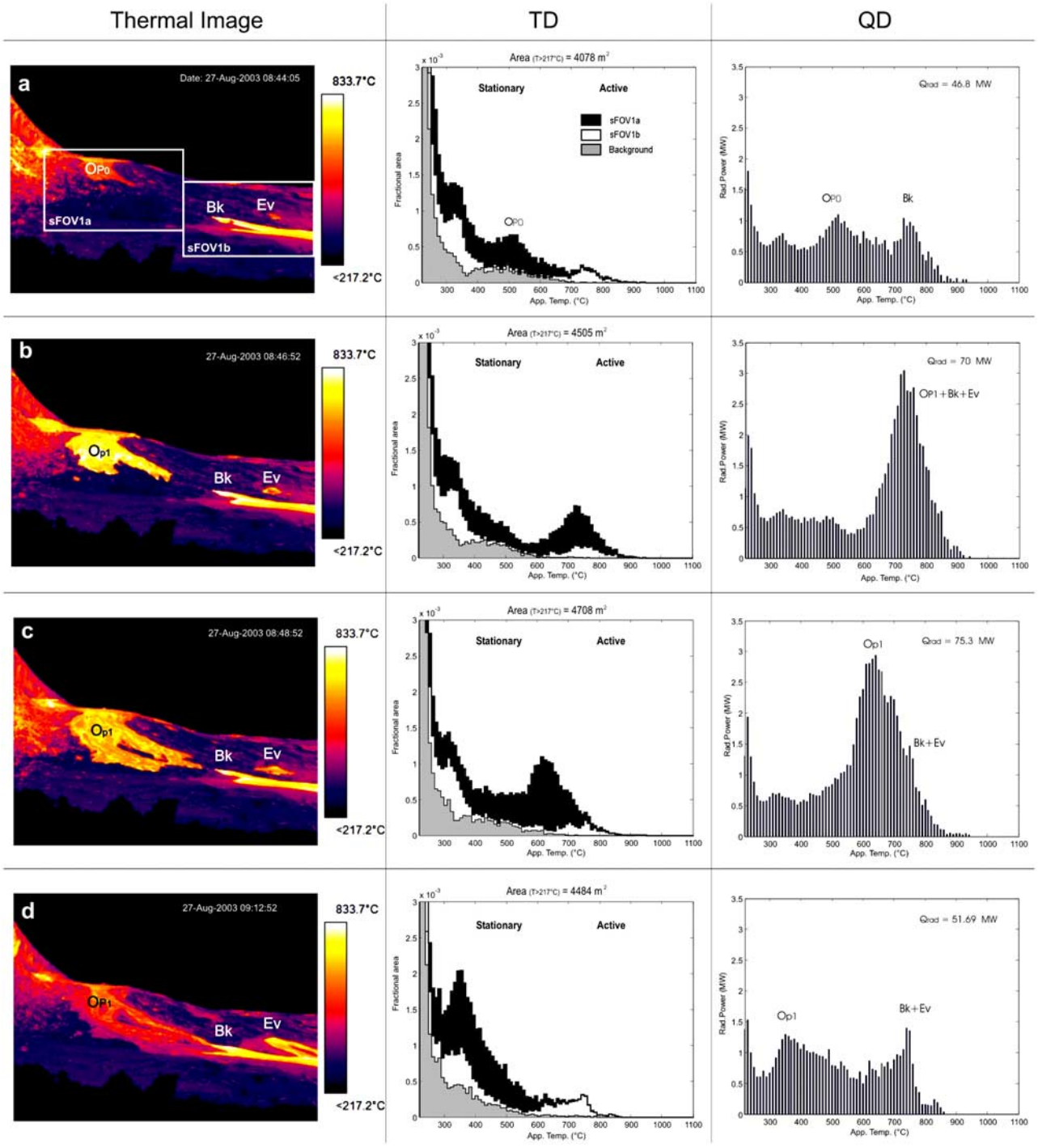

Figure 10. Thermal images, TD, and QD during the pulse P1: (a) before the pulse two main components represents a older lava pond overflow (O_{P0}) and the active Bk; (b) P1 generates a new overflow (O_{P1}) and the opening of Ev, whose thermal components overlap the Bk component in the active region; (c) once the pulse ceased, the overflow cools and its component ''move'' toward the stationary region. The Bk and Ev components are persisting in the active region; (d) the overflow cooled down (its component is being absorbed by the background), and the Bk and Ev components have increased their activity.

cooling rate acting on the associated surfaces; the fall of tephra (lapilli and spatters) within the FOV is represented by steeper curves (Lpf) related to rapid cooling acting on the dispersed material.

[56] The length of the anomalies is function of the duration of the event. For example, pulse P1 (08:45) produced the emission of new lava by overflowing the barrier (lasting for a few minutes) and was followed by continuous opening of several ephemeral vents (Ev_{1a}, Ev_{1b},

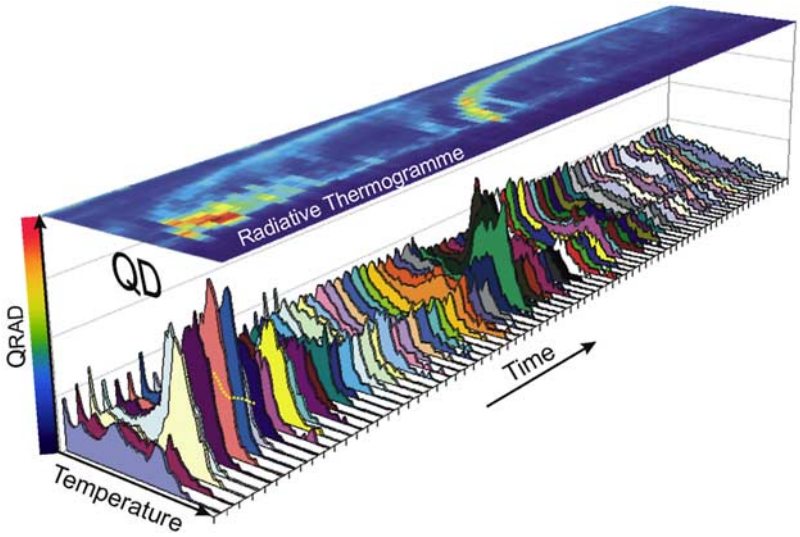

Figure 11. Three-dimensional image for the construction of the radiative thermogramme (named "RadTherm") The QD are placed side by side and their intensity is represented according to a logarithmic color scale of the radiative heat flux (Q_{Rad}).

and Ev_{1c}), a process that lasted for more than 30 min (thermal components persist in the active region at high energy levels until 09:29). Pulse P2 (09:47) lasted few minutes as well, but in this case, the overflow (O_{P2}) was followed by more discontinuous opening of small ephemeral vents (Ev_{2a}, Ev_{2b}, Ev_{2c}, and Ev_{2d}).

[57] The "RadTherm" illustrated in Figure 12a shows also that the intensity associated to the persistent activity of the main Bk and the Ev decreased with time. In this case, we may observe a gradual decrease of the bulk radiative energy within the active region, but there is no shifting toward lower temperatures. On the contrary, the "cooler limit" of this component is still within the active region of the "RadTherm" and gradually moves toward higher temperatures. This is likely due to the "roofing process" that is reducing the area of the exposed moving surface within the FOV during the periods between two pulses. It is unlikely that this phenomenon is associated to a decrease in the channel flow rate. Rather, it seems to be related to the displacement of Bk because of the onset and development of a new roofing process.

[58] On the contrary, the highest temperature domains (which is associated to the maximum recorded temperature within the FOV) show that the active component slowly moves toward hotter temperatures (at least until the onset of pulse P3 at 11:35). This is consistent with field observations, since lava effusion at the base of the cone slightly increased within this span of time.

[59] The "RadTherm" of FOV2 is reported in Figure 12b. The main features in this figure is the presence of a persistent thermal component (with higher radiative flux) related to the hot lava flowing within the open channel.

[60] The occurrence of pulse P4 caused the increase of the lava pond level, followed by channel overflows at 13:35. This event is associated with the increase of thermal components within the active region, coupled with the coeval onset of a typical cooling curve (O_{Ch4}), which is related to the emplacement and cooling of lateral thin pahoehoe sheets.

[61] Minor events were detected before the major pulse P5. These minor pulses (named P4a, P4b, and P4c) were due to the squeezing of lava from ephemeral vents and consequent cooling (as shown by curves Ev_{4a}, Ev_{4b}, and Ev_{4c}). The relatively high temperature peak recorded at 14:35 is related to the breaking of the roof with the exposure of the flow interior.

[62] Unfortunately, the onset of pulse P5 (that cause a marked lava-pond overflow) was not enclosed in the field of view during our monitoring. However, we only recorded channel overflows downstream at 15:59, where we were standing (Figure 12b on the right). It is interesting to notice that a couple of minutes later, the slight decrease in temperatures in the active region during and right after its onset are "counterbalanced" by the increase in radiative power due to overflow (O_{Ch5}) in the stationary region. This effect is likely due to the entering within the FOV of the cooling lava flow produced by the pond's overflow associated to P5.

[63] The "RadTherm" of FOV3 (Figure 12c) shows again the intensity of the active components due to the active breakout coupled with the occurrence of minor pulses (Ev_{5b} ,Ev_{5c}, and Ev_{5d}) and fall of lapilli and scoriae (Lpf) on the flank of the vent. Pulse P6 is marked by the pond overflow (O_{P6}) and by the related cooling curve. Following the end of the eruption, we observed minor flowing from the lava pond associated with draining (that persisted for approximately 15 min).

6. Thermal and Seismic Activity

[64] The "RadTherm" of the whole sequence (Figure 13a) allowed us to calculate the total radiative heat flux lost by the monitored portion of the lava field (Figure 13b).

[65] During steady state effusion, the monitored portion of lava channel radiated with an average value of about 60 MW (Figure 13b, FOV2). Despite the fact that this analyzed area (about 2000 m^2) represents only the 0.125% of the whole flow field area, the associated radiative heat flux correspond to 1–3% than those estimated, for the entire

flow field by using the MODVOLC data (2000–6000 MW; Figure 3). This suggests that the rest of the flow field does not irradiate as high as the monitored portion of lava channel located in proximity of the vent. During the pulsing episodes, the effusion rate increased nearly instantaneously more than 100% with respect to its averaged value (from 14 ± 6 m^3/s during the steady state conditions up to 34 ± 10 m^3/s during the pulses). These events were accompanied by peaks

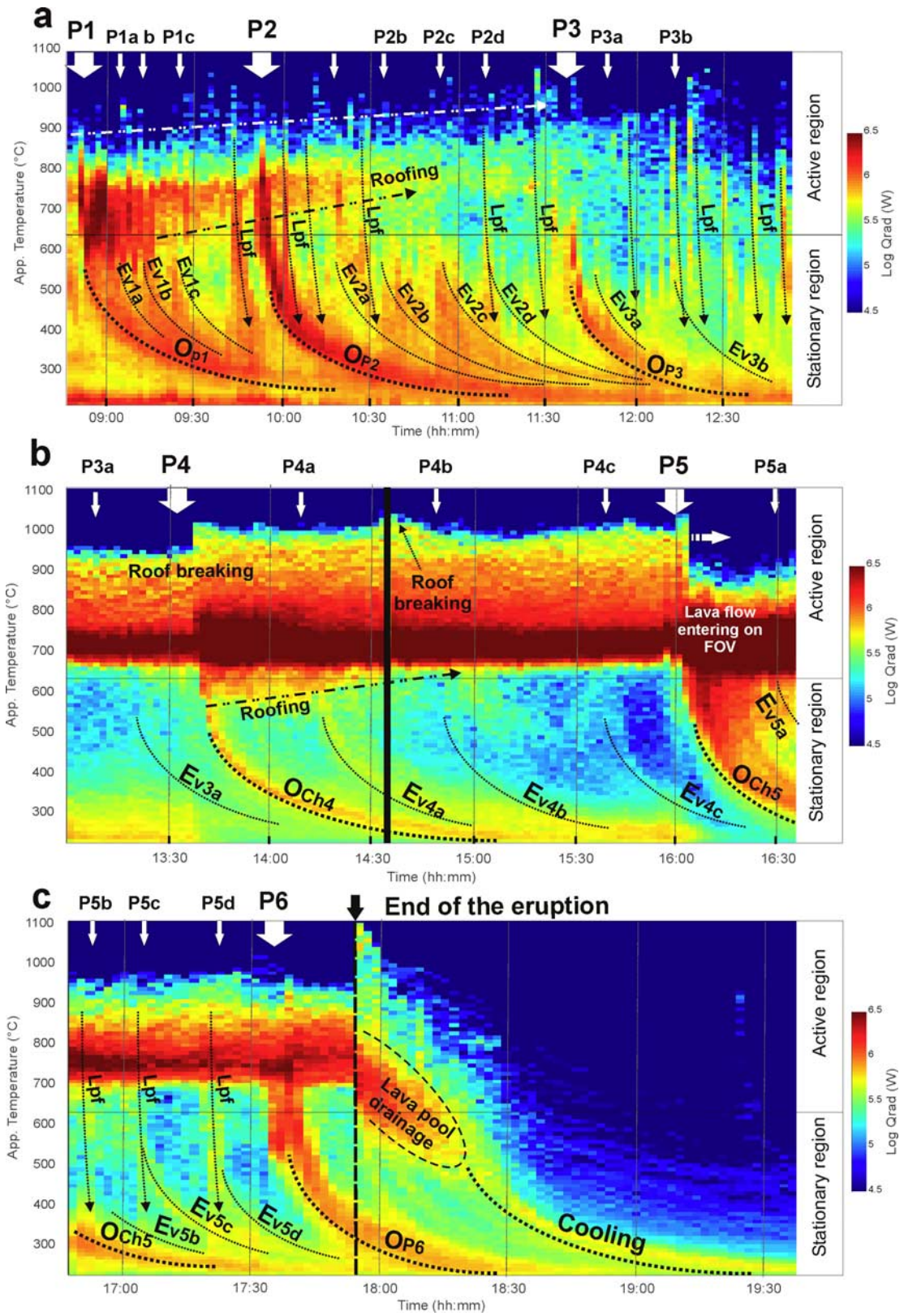

Figure 12

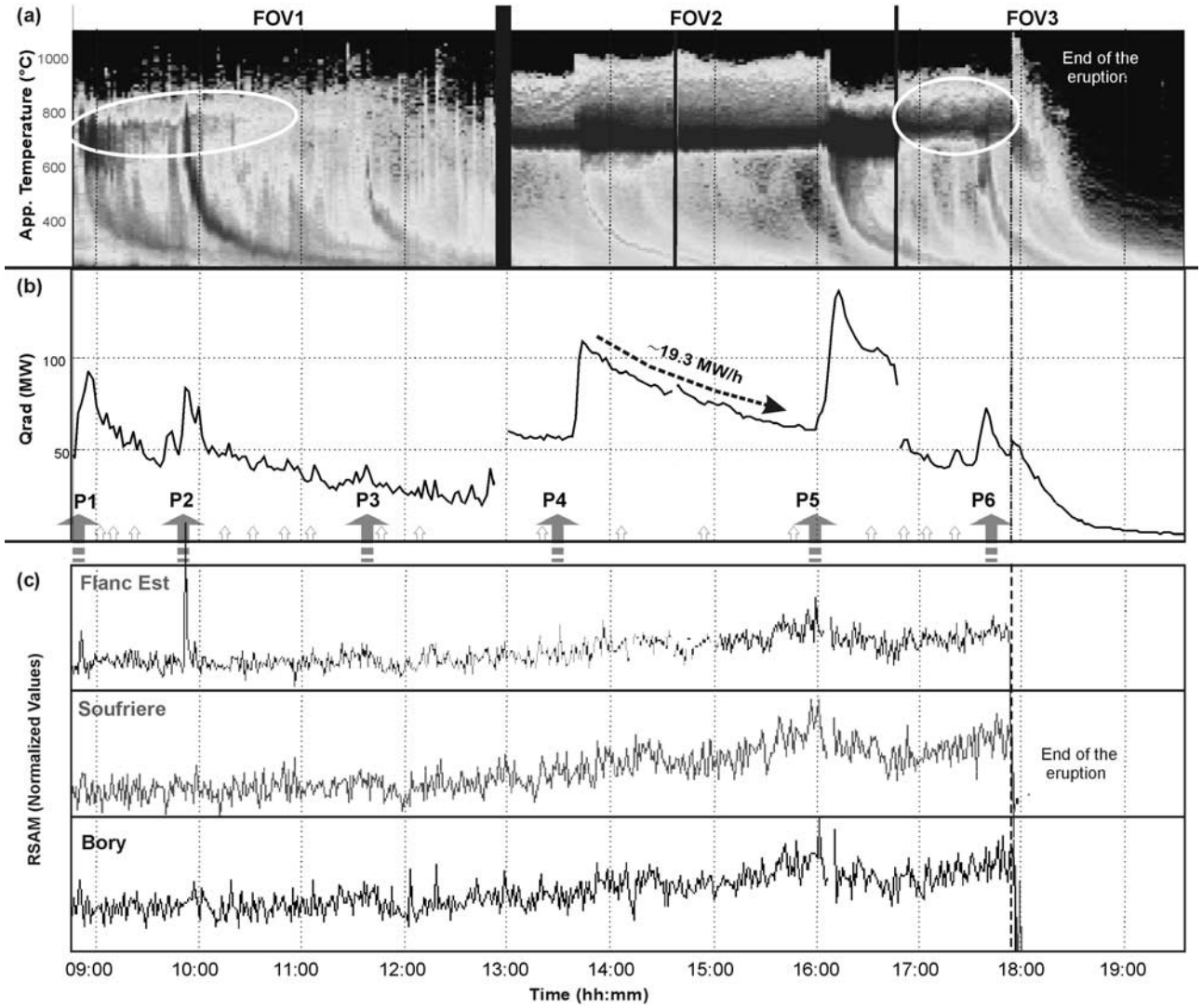

Figure 13. Synthesis of thermal data recorded on 27 August 2003, compared with seismic records (a) "RadTherm" of the whole sequence; (b) Radiative heat flux (Q_{Rad}) derived from the "RadTherm"; major peaks correspond to the occurrence of pulses episodes. The roofing process causes a marked decrease in the heat radiated by the flow surface; (c) RSAM (1 min) recorded at three seismic stations (data provided by the Observatoire Volcanologique du Piton de la Fournaise).

of the radiative heat flux of about 50–80 MW above the steady emission (Figure 13b) or rather about 1–4% of the MODIS-derived heat flux. These relative small "thermal pulses" are not proportional to the intensity of the associated "effusive pulses," likely because of the short duration of the event coupled with the reduced amount of area involved during the emplacement of the new lava (about 0.2% of the whole flow field). Consequently, important but very quick pulses in the effusion rate produce less evident anomalies of the thermal radiation detectable from satellite.

[66] Observing the active component at the beginning (FOV1) and the end (FOV3) of the "RadTherm" (evidenced with white ellipses in Figure 13a), we point out the occurrence of a shift toward higher temperatures coupled with a

Figure 12. "RadTherm" of 27 August 2003 thermal data for FOV1, FOV2, and FOV3, respectively, (a) the occurrence of pulse P1, P2, and P3 is marked by the increase in radiative energy from the active region and by the cooling of the lava-pond overflows (O_P). Minor anomalies are due to the opening of Ev or lapilli fall-out (Lpf); (b) The major energetic component in the active region is due to the high activity on the channel surface on FOV2. Here pulses (P4 and P5) generate channel overflows and the related cooling curves (O_{Ch}). The squeezing of molten lava from ephemeral vents is represented by minor cooling curves on the lower part of the thermogramme. (c) Following pulse (P6), the end of the eruption is accompanied by a sudden energy decrease. This is related to the drainage of the lava pond with a gradual shift of the temperatures toward lower values followed by a typical cooling trend.

general increase of the radiative heat flux released by the breakout and the ephemeral vents at the base of the cone. This suggests a slight increase of the effusion rate that is also supported by the trend of the tremor intensity (RSAM 1 min) recorded by three seismic stations (Figure 13c).

[67] The cross-check of the radiative flux with the tremor amplitude data show that most of the effusive pulses have been recorded as anomalies by the seismic stations. Some of the major pulses were coeval with recorded spikes of volcanic tremor (P1, P2, P4, and P5), whereas pulses P3 and P6 occurred during an increasing trend in tremor intensity followed by a short period of decrease.

[68] As previously mentioned, we suggest that these cyclic pulses were associated to the occurrence of gas piston events. This is supported by the following field observations:

[69] 1. During our infrared monitoring (lasting approximately 10 hours), we never observed collapses of the crater wall. Therefore this phenomenon was not involved in triggering the changes of the lava level within the pond.

[70] 2. Since the main Bk drained continuously and almost steadily the lava pond, we exclude that the increased level of magma within the cone resulted from an obstruction developed in the conduit feeding the lava channel.

[71] 3. The effusive pulses were coupled with an increase in the fountains' height; thus suggesting the occurrence of some degassing process within the feeding system and/or the conduit.

[72] Generally, gas piston events occur when the magma column is cyclically pushed up within the conduit by rising gas bubbles [*Johnson et al.*, 2005]. Such a process is accompanied by periodic variations of the tremor amplitude [*Chouet and Shaw*, 1991; *Ferrazzini et al.*, 1991] and eventually by cyclic episodes of inflation [*Barker et al.*, 2003]. The pulses observed at Piton Payankë occurred within a very active and degassing lava pond and were associated to anomalies in the tremor amplitude. Although the observed gas piston events did not produce the typical cigar-shaped envelope of volcanic tremors [*Ferrazzini et al.*, 1991], their seismic signature can be largely masked by the interference of high-amplitude seismic signal due to the high effusion rates and vigorous fountaining at the vent. Moreover, changes in fountains' heights can be associated with the arrivals (up the surface) of distinct gas slugs and/or with the arrival of highly foamy magma distributed into large 'pockets' within the ascending magma column, as suggested by *Jaupart and Vergniolle* [1989].

[73] According to *Johnson et al.* [2005], we may classify the effusive pulses observed at Piton Payankë as gas piston events of type II. These are characterized by the initial extrusion of molten lava, followed by the expansion and the release of gas and ejecta once the slugs and/or foamy magma reach the free surface.

7. Conclusions

[74] The alternation of a steady state effusion with dynamic effusive pulses in the vent area produced thermal patterns that may be used to better evaluate and eventually calibrate remotely achieved thermal anomalies observed from satellites. In particular, marked and rather instantaneous peaks in the effusion rate (eventually associated to gas pistons events) can be represented by reduced thermal anomalies (especially if they involve a small area for a short time). Therefore these anomalies may be relatively small when compared with the average radiative heat flux (and hence the effusion rate) estimated from satellite [*Wright et al.*, 2001].

[75] Conversely, a gradual decrease of the radiative heat flux can result from roofing processes and may not necessarily be related to changes in the effusion rate. We estimate that during steady state conditions, the roofing process can reduce the radiation released by the flow field of nearly 19.3 MW/h (see the average slope of Figure 13b). This relatively high value gives a significant clue for better understanding thermal anomalies, especially for long-lived steady state eruptions that normally develop lava tubes.

[76] Finally, we propose a new method for the analysis of thermal data collected on active volcanoes that can be easily correlated with other monitoring data. In our view, the use of the RadTherm is a promising and potentially useful way to visualize field thermal data, since it can effectively discriminate the onset and the evolution of several coeval dynamic processes such as overflows, roofing process, tephra fallout, decreasing lava supply rates, extensive cooling, and so on. We suggest that with appropriate field measurements, it will possible to apply the "RadTherm" to better detect the difference in the cooling rate of a variety of volcanic structures and/or material (including tephra, bombs, blocks, and expanding volcanic gases). In the short run, the applications of these methods in real-time monitoring could lead to a significant improvement of volcano surveillance.

[77] **Acknowledgments.** D. Coppola's work was funded by the European Volcano Dynamics Research Training Network and by GNV-INGV Research Fellowship. We acknowledge Valerie Ferrazini who provided the seismic data, Philippe Catherine and Philippe Kowalsky who helped us during fieldwork. Instrumental and logistic support was kindly given by the "Observatoire Volcanologique du Piton de la Fournaise". We acknowledge the MODIS Alert Team (http://modis.higp. hawaii.edu/) who provided MODVOLC data. L. Wesley reviewed the English.

References

Albaréde, F., B. Luais, G. Fitton, M. Semet, E. Kaminski, B. G. J. Upton, P. Bachelery, and J. L. Cheminée (1997), The geochemical regimes of Piton de la Fournaise Volcano (Réunion) during the last 530,000 years, *J. Petrol.*, *38*(2), 171–201.

Bailey, J. E., A. J. L. Harris, J. Dehn, S. Calvari, and S. K. Rowland (2006), The changing morphology of an open lava channel on Mt Etna, *Bull. Volcanol.*, *68*, 497–515, doi:101007/s00445-005-0025-6.

Ball, M., and H. Pinkerton (2006), Factrors affecting the accuracy of thermal imaging cameras in volcanology, *J. Geophys. Res.*, *111*, B11203, doi:10.1029/2005JB003829.

Barker, S. R., D. R. Sherrod, M. Lisowski, C. Heliker, and J. S. Nakata (2003), Correlation between lava-pond drainback, seismicity, and ground deformation at Pu'u'O' o, in *The Pu'u'O' o-Kupaianaha Eruption of Kilauea Volcano, Hawaii: The First 20 Years*, edited by C. Heliker, D. A. Swanson, and T. J. Takahashi, *U.S. Geol. Surv. Prof. Pap.*, 1676, 53–62.

Battaglia, J., K. Aki, and T. Staudacher (2005), Location of tremor sources and estimation of lava output using tremor source amplitude on the Piton de la Fournaise volcano: 2. Estimation of lava output, *J. Volcanol. Geotherm. Res.*, *147*, 291–308.

BGVN (1998), Piton de la Fournaise, *Bulletin of the Global Volcanism Network*, *23*(3).

BGVN (2000), Piton de la Fournaise, *Bulletin of the Global Volcanism Network*, *25*(7).

BGVN (2001), Piton de la Fournaise, *Bulletin of the Global Volcanism Network*, *26*(5).

BGVN (2003), Piton de la Fournaise, *Bulletin of the Global Volcanism Network*, *28*(8).

Calvari, S., and T. Pinkerton (2004), Birth, growth and morphologic evolution of the 'Laghetto' cinder cone during the 2001 Etna eruption, *J. Volcanol. Geotherm. Res.*, *132*, 225–239.

Calvari, S., L. Spampinato, L. Lodato, A. J. L. Harris, M. R. Patrick, J. Dehn, M. R. Burton, and D. Andronico (2005), Chronology and complex volcanic processes during the 2002-2003 flank eruption at Stromboli volcano (Italy) reconstructed from direct observations and surveys with a handheld thermal camera, *J. Geophys. Res.*, *110*, B02201, doi:10.1029/2004JB003129.

Chouet, B. A., and H. R. Shaw (1991), Fractal properties of tremor and gas piston events observed at Kilauea Volcano, Hawaii, *J. Geophys. Res.*, *96*, 10,177–10,189.

Coppola, D., T. Staudacher, and C. Cigolini (2005), The May-July eruption at Piton de la Fournaise (La Réunion): volume, effusion rates and emplacement mechanisms inferred by thermal imaging and GPS survey, In M. Manga and G. Ventura (Eds), Kynematics and dynamics of lava flows, *Gelogical Society of America Special Paper* 396, pp. 103-124.

Donegan, S. J., and L. P. Flynn (2004), Comparison of the response of the Landsat 7 Enhanced Thematic Mapper Plus and the Earth Observing-1 Advanced Land Imager over active lava flows, *J. Volcanol. Geotherm. Res.*, *135*, 105–126.

Ferrazzini, V., K. Aki, and B. A. Chouet (1991), Characteristics of seismic waves composing Hawaiian volcanic tremor and gas-piston events observed by a near-source array, *J. Geophys. Res.*, *96*, 6199–6209.

Flynn, L. P., and P. J. Mouginis-Mark (1992), Cooling rate of an active Hawaiian lava flow from nighttime spectroradiometer measurements, *J. Geophys. Res.*, *19*, 1783–1786.

Flynn, L. P., and P. J. Mouginis-Mark (1994), Temperature of an active lava channel from spectral measurements, Kilauea Volcano, Hawaii, *Bull. Volcanol.*, *56*, 297–301, doi:101007/BF00302082.

Flynn, L. P., P. J. Mouginis-Mark, J. C. Gradie, and P. G. Lucey (1993), Radiative temperature measurements at Kupaianaha Lava Lake, Kilauea Volcano, Hawaii, *J. Geophys. Res.*, *98*, 6461–6476.

Flynn, L. P., P. J. Mouginis-Mark, and K. A. Horton (1994), Distribution of thermal area on an active lava flow field: Landsat observation of Kilauea, Hawaii, July 1991, *Bull. Volcanol.*, *56*, 284–296.

Francis, P. W., and D. A. Rothery (1987), Using the Landsat Thematic Mapper to detect and monitor active volcanoes: An example from Lascar volcano, northern Chile, *Geology*, *15*, 614–617.

Froger, J. L., Y. Fukushima, P. Briole, Th. Staudacher, T. Souriot, and N. Villeneuve (2004), The deformation field of the August 2003 eruption at Piton de la Fournaise, Reunion Island, mapped by ASAR interferometry, *Geophys. Res. Lett.*, *31*, L14601, doi:10.1029/2004GL020479.

Griffiths, R. W. (2000), The dynamics of lava flows, *Annu. Rev. Fluid Mech.*, *32*, 477–518.

Griffiths, R. W., R. C. Kerr, and K. V. Cashman (2003), Patterns of solidication in channel flows with surface cooling, *J. Fluid Mech.*, *496*, 33–62, doi:10.1017/S0022112003006517.

Harris, A. J. L., and A. J. H. Maciejewski (2000), Thermal surveys of the Vulcano Fossa fumarole field 1994–1999: Evidence for fumarole migration and sealing, *J. Volcanol. Geotherm. Res.*, *102*, 119–147.

Harris, A. J. L., N. F. Stevens, A. J. H. Maciejewski, and P. J. Rollin (1996), Thermal evidence for linked vents at Stromboli, *Acta Vulcanologica*, *8*, 57–62.

Harris, A. J. L., A. L. Butterworth, R. W. Carlton, I. Downey, P. Miller, P. Navarro, and D. A. Rothery (1997), Low-cost volcano surveillance from space: case studies from Etna, Krafla, Cerro Negro, Fogo, Lascar and Erebus, *Bull. Volcanol.*, *59*, 49–64.

Harris, A. J. L., J. B. Murray, S. E. Aries, M. A. Davies, L. P. Flynn, M. J. Wooster, R. Wright, and D. A. Rothery (2000), Effusion rate trends at Etna and Krafla and their implications for eruptive mechanisms, *J. Volcanol. Geotherm. Res.*, *102*, 237–269.

Harris, A. J. L., L. P. Flynn, O. Matias, and W. I. Rose (2002), The thermal stealth flows of Santiaguito: Implications for the cooling and emplacement of dacitic block lava flows, *Geol. Soc. Am. Bull.*, *114*(5), 533–546.

Harris, A. J. L., J. Bailey, S. Calvari, and J. Dehn (2005a), Heat loss measured at a lava channel and its implications for down-channel cooling and rheology, in *Kynematics and Dynamics of Lava Flows*, edited by M. Manga and G. Ventura, *Gelogical Society of America Special Paper*, *396*, pp. 125–146.

Harris, A. J. L., R. Carniel, and J. Jones (2005b), Identification of variable convective regimes at Erta Ale lava lake, *J. Volcanol. Geotherm. Res.*, *142*, 207–223.

Harris, A. J. L., J. Dehn, M. Patrick, S. Calvari, M. Ripepe, and L. Lodato (2005c), Lava effusion rates from hand-held thermal infrared imagery: An example from the June 2003 effusive activity at Stromboli, *Bull. Volcanol.*, *68*, 107–117.

Hon, K., J. Kauahikaua, R. Denlinger, and K. McKay (1994), Emplacement and inflations of pahoeohe sheet flows: observations and measurements of active lava flows on Kilauea Volcano, Hawaii, *Geol. Soc. Am. Bull.*, *106*, 351–370.

James, M. R., S. Robson, H. Pinkerton, and M. Ball (2006), Oblique photogrammetry with visible and thermal images of active lava flows, *Bull. Volcanol.*, *69*, 105–108, doi:101007/s00445-006-0062-9.

Jaupart, C., and S. Vergniolle (1989), The generation and collapse of a foam layer at the roof of a basaltic magma chamber, *J. Fluid Mech.*, *203*, 347–380.

Johnson, J. B., A. J. L. Harris, and R. P. Hoblitt (2005), Thermal observations of gas pistoning at Kilauea Volcano, *J. Geophys. Res.*, *110*, B11201, doi:10.1029/2005JB003944.

Kaneko, T., M. J. Wooster, and S. Nakada (2002), Exogenous and andogenous growth of the Unzen lava dome examined by satellite infrared image analysis, *J. Volcanol. Geotherm. Res.*, *116*, 151–160.

Keszthelyi, L., and R. Denlinger (1996), The initial cooling of pahoehoe flow lobes, *Bull. Volcanol.*, *58*, 5–18.

Peltier, A., V. Ferrazzini, T. Staudacher, and P. Bachelery (2005), Imaging the dynamics of dyke propagation prior to the 2000-2003 flank eruptions at Piton de La Fournaise, Reunion Island, *Geophys. Res. Lett.*, *32*, L22302, doi:10.1029/2005GL023720.

Peltier, A., T. Staudacher, and P. Bachèlery (2006), Constraints on magma transfers and structures involved in the 2003 activity at Piton de La Fournaise from displacement data, *J. Geophys. Res. solid earth*.

Peterson, D. W., R. T. Holcomb, R. I. Tilling, and R. L. Christiansen (1994), Developement of lava tubes in the light of observations at Mauna Ulu, Kilauea volcano, Hawaii, *Bull. Volcanol.*, *56*, 343–360.

Pieri, D. C., L. S. Glaze, and M. J. Abrams (1990), Thermal radiance observations of an active lava flows during the June 1984 eruption of Mount Etna, *Geology*, *18*, 1018–1022.

Pinkerton, H., M. James, and A. Jones (2002), Surface temperature measurement of active lava flows on Kilauea volcano, Hawai'I, *J. Volcanol. Geotherm. Res.*, *113*, 159–176.

Rothery, D. A., P. W. Francis, and C. A. Wood (1988), Volcano monitoring using short wavelength infrared data from satellites, *J. Geophys. Res.*, *93*, 7993–8008.

Staudacher, T., K. Aki, P. Bachèlery, P. Catherine, V. Ferrazzini, D. Hochard, P. Kowalski, L. P. Ricard, N. Villeneuve, and J. L. Cheminée (2001), New eruption cycle at Piton de la Fournaise Volcano, Réunion Island, *European Geophysical Society, News Letter*, *78*, 80.

Staudacher, T., L. Ruzié, and A. Peltier (2007), *Historique des Éruptions du Piton de la Fournaise de 1998 à 2006*, OVPF/IPGP edition, 84.

Swanson, D. A., W. A. Duffield, D. B. Jackson, and D. W. Peterson (1979), Chronological narrative of the 1969- 71 Mauna Ulu eruption of Kilauea Volcano, Hawaii, *U.S. Geol. Surv. Prof. Pap.*, *1056*, 55 pp.

Tilling, R. I. (1987), Fluctuations in surface height of active lava lakes during 1972–1974 Mauna Ulu eruption, Kilauea Volcano, Hawaii, *J. Geophys. Res.*, *92*, 13,721–13,730.

Vlastélic, I., T. Staudacher, and M. Semet (2005), Rapid change of lava composition from 1998 to 2002 at Piton de la Fournaise (Réunion) inferred from Pb isotopes and trace elements: Evidence for variable crustal contamination, *J. Petrol.*, *46*(1), 79–107.

Wright, R., and L. Flynn (2003), On the retrieval of lava-flow surface temperatures from infrared satellite data, *Geology*, *3*(10), 893–896.

Wright, R., and L. Flynn (2004), Space-based estimate of the volcanic heat flux into the atmosphere during 2001 and 2002, *Geology*, *32*(3), 189–192.

Wright, R., S. Blake, A. J. L. Harris, and D. A. Rothery (2001), A simple explanation for the space-based calculation of lava eruption rates, *Earth Planet. Sci. Lett.*, *192*, 223–233.

Wright, R., L. Flynn, H. Garbeil, A. J. L. Harris, and E. Pilger (2002), Automated volcanic eruption detection using MODIS, *Remote Sens. Environ.*, *82*, 135–155.

Wright, R., L. Flynn, H. Garbeil, A. J. L. Harris, and E. Pilger (2004), MODVOLC: Near-real-time thermal monitoring of global volcanism, *J. Volcanol. Geotherm. Res.*, *135*, 29–49.

C. Cigolini and D. Coppola, Dipartimento di Scienze Mineralogiche e Petrologiche, Università di Torino, Via Valperga Caluso 35, 10125, Torino, Italy. (corrado.cigolini@unito.it; diego.coppola@unito.it)

T. Staudacher, Observatoire Volcanologique du Piton de la Fournaises, Institut de Physique du Globe de Paris, UMR 7154, 14 RN3, le 27Km, 97418 La Plaine des Cafres, La Réunion, France. (thomas.staudacher@univ-reunion.fr)